

**Light emission of sonoluminescent bubbles containing a rare gas and water vapor**

Dominik Hammer and Lothar Frommhold

*Department of Physics, The University of Texas at Austin, Austin, Texas 78712*

(Received 30 November 2001; published 11 April 2002)

We present numerical simulations of sonoluminescent rare-gas bubbles in water, which account for (i) time variations of the water vapor content, (ii) chemical reactions, and (iii) the ionization of the rare gas and the  $\text{H}_2\text{O}$  dissociation products. Peak temperatures exceed 10 000 K at densities of a few hundred amagat ( $\approx 10^{28}$  particles per  $\text{m}^3$ ). The gas mixture in the bubble is weakly ionized. Our model accounts for the light emission by electron-atom, electron-ion, and ion-atom bremsstrahlung, recombination radiation, and radiative attachment of electrons to hydrogen and oxygen atoms, which are all more or less important for single bubble sonoluminescence. Spectral shapes, spectral intensities, and durations of the light pulses are computed for helium, argon, and xenon bubbles. We generally obtain good agreement with the observations for photon numbers and pulse durations. Some calculated spectral profiles agree, however, less well with observations, especially in the case of the low water temperature and for helium bubbles. We try to identify the reasons why computed and observed spectral profiles might discernibly differ when all other computed features considered here seem to be quite consistent with observations. We show that by allowing the bubble to heat somewhat nonisotropically, agreement between observed and computed spectral profiles may be obtained, even in the case of helium bubbles at freezing water temperatures. In this case, charge exchange radiation and related processes involving helium atoms and ions become important.

DOI: 10.1103/PhysRevE.65.046309

PACS number(s): 78.60.Mq, 41.60.-m, 52.25.Os

**I. INTRODUCTION**

Sonoluminescence is the conversion of sound energy into light. In recent years this phenomenon has been studied quite intensely, especially since single bubble sonoluminescence was discovered [1]. Many more or less sophisticated models have been suggested to explain the surprising phenomena of luminescence induced by cavitation [2–10]. A reasonably realistic and quite successful description is the weakly ionized gas model [9–15]. In this model, the gas in the bubble is heated quasiadiabatically to roughly 10 or 20 000 K. Owing to the high densities of the sonoluminescent environment only about a few percent of the gas is ionized at these temperatures. Several well-known radiative processes contribute to the emission of light under such conditions, for example, bremsstrahlung arising from collisions of electrons with atoms or ions, and from radiative attachment or recombination. The weakly ionized gas model describes the observed photon numbers, the duration of the light flashes, and their dependence on each other and on the experimentally adjustable parameters closely in the case of the heavier rare-gas bubbles [12]. In these cases spectral shapes of the emitted light in close agreement with the observations have also been reported [15].

However, the model as presented in Refs. [12,15] has two significant shortcomings. First, it incorrectly predicts that at low driving frequencies ( $< 10$  kHz) much more light should be emitted than at the widely used higher sound frequencies (20–30 kHz) [16]. Second, especially in the case of helium bubbles, it fails to reproduce the observed intensities [12]. It has been argued [17] that the first problem is likely to be solved by accounting for the varying water vapor content of the bubble during expansion and compression.

We show here that a hydrodynamic model that includes a

treatment of water vapor helps to lessen the second problem as well. We account for condensation and evaporation of the water vapor; include a detailed treatment of its chemistry; compute ionization of the gas mixture from ionization rate equations; and take into account several well-known radiative processes, some of which have not been considered in the existing models of the sonoluminescent emission. While our main interest is the light generation, we also considered simple modifications to the equation of state, looked at the model of  $\text{H}_2\text{O}$  chemistry, and corrected the treatment of the ionization process. Our extended model describes light intensities and pulse widths in accordance with the observations made under various experimental conditions with rare-gas bubbles. Moreover, some of the spectral profiles computed compare favorably with observation, yet other spectral profiles, especially those computed for freezing water temperature and helium bubbles, differ. Calculated profiles show excess intensity in the red but are somewhat deficient in the ultraviolet while the integrated intensities are consistent with observations. In an attempt to identify the reasons for such differences, we show that by allowing the bubble to heat somewhat nonuniformly, agreement between observed and computed spectral intensity distributions may be obtained, even for helium bubbles in freezing water.

**II. HYDRODYNAMIC MODELING****A. Rayleigh-Plesset equation and equation of state**

We assume a spatially uniform bubble filled with a mixture of rare gas and water vapor. The radius of the bubble  $R(t)$  as function of time  $t$  is obtained from a variant of the Rayleigh-Plesset equation [17–19],

$$\begin{aligned} & \left(1 - \frac{\dot{R}}{c_l}\right) \ddot{R} R + \frac{3}{2} \left(1 - \frac{\dot{R}}{3c_l}\right) \dot{R}^2 \\ &= \frac{1}{\rho_l} \left[ \left(1 + \frac{\dot{R}}{c_l}\right) [p - P_s(t) - P_0] + \frac{R}{c_l} \dot{p}_g - 4\eta_l \frac{\dot{R}}{R} - \frac{2\sigma_l}{R} \right]. \end{aligned} \quad (1)$$

Here  $c_l$  is the speed of sound,  $\rho_l$  is the density,  $\eta_l$  is the viscosity, and  $\sigma_l$  is the surface tension of liquid water, all determined at the ambient water temperature  $T_\infty$ . The applied sound field  $P_s(t)$  of amplitude  $P_a$  and frequency  $\omega_a$  is given by  $-P_a \cos(\omega_a t)$  and the pressure  $p$  of the gas in the bubble at temperature  $T$  is given by a van der Waals type equation of state,

$$p(t) = \frac{[N_{\text{tot}}(t) + N_e(t)] k_B T(t)}{V'(t)}, \quad (2)$$

with the free volume  $V'$ ,

$$V'(t) = \frac{4\pi}{3} R(t)^3 - \sum_i b_i N_i(t). \quad (3)$$

The summation is over all species of atoms and molecules  $i$  in the bubble with their excluded volume  $b_i$  (in  $\text{m}^3$  per atom or molecule) and their number  $N_i(t)$  present in the bubble; the same  $b_i$  is used for the neutral or ionized state<sup>1</sup> of species  $i$ .  $N_{\text{tot}}(t) = \sum_i N_i(t)$  and  $N_e(t)$  is the number of electrons at time  $t$ .

### B. Evaporation and condensation of water

The number  $N_{\text{tot}}$  of particles in the bubble varies in time due to chemical reactions of water vapor (to be detailed below) and the evaporation and condensation of water molecules at the bubble wall,

$$\dot{N}_{\text{H}_2\text{O}}^{\text{wall}}(t) = 4\pi R(t)^2 J(t). \quad (4)$$

The radial molecular flux into the bubble through the bubble surface is given by [11,20–22]

$$J(t) = \frac{\alpha_M}{\sqrt{2\pi m_{\text{H}_2\text{O}} k_B}} \left( \frac{p_{\text{H}_2\text{O}}^{\text{vap}}}{\sqrt{T_\infty}} - \frac{\Gamma(t) p_{\text{H}_2\text{O}}(t)}{\sqrt{T(t)}} \right). \quad (5)$$

The accommodation coefficient  $\alpha_M$  for water molecules on the bubble surface is set to the value corresponding to  $T_\infty$ ,  $\alpha_M = 0.35$  [11]. The partial pressure of water molecules of mass  $m_{\text{H}_2\text{O}}$  in the bubble is  $p_{\text{H}_2\text{O}}(t) = p(t) N_{\text{H}_2\text{O}}(t) / N_{\text{tot}}(t)$  and  $p_{\text{H}_2\text{O}}^{\text{vap}}$  is the (saturated) water vapor pressure at the ambient temperature  $T_\infty$ . The factor  $\Gamma$  corrects for the fact that

<sup>1</sup>The excluded volume  $b_i$  of positive ions is actually smaller than that of the parent atom, because of Coulomb contraction. Such detail seems, however, not particularly significant, owing to the relatively small ion concentrations.

only a certain fraction of the gas molecules in the bubble actually moves towards the bubble interface,

$$\Gamma = \exp(-\Omega^2) - \Omega \sqrt{\pi} [1 - \text{erf}(\Omega)], \quad (6)$$

with

$$\Omega = \frac{J}{p_{\text{H}_2\text{O}}} \sqrt{\frac{m_{\text{H}_2\text{O}} k_B T}{2}}. \quad (7)$$

For most of the acoustic cycle the derivatives of  $\text{H}_2\text{O}$  exist in only small concentrations so that their loss or gain may be neglected and the number of rare-gas atoms is assumed to be constant since only bubbles in stable diffusive equilibrium are considered in this paper.

### C. Energy balance

Temperatures in the bubble are determined mostly by adiabatic heating, but heat loss to the surrounding water cannot be ignored. Furthermore, the chemical reactions, Eq. (18) below, as well as ionization reactions, consume a substantial amount of energy. An energy loss of  $\eta \approx \frac{8}{2} k_B T_\infty$  [17] is associated with each water molecule condensing out of the bubble. Thus the change of the internal energy  $E$  of the bubble is given by

$$\dot{E}(t) = \eta \dot{N}_{\text{H}_2\text{O}}^{\text{wall}}(t) + \dot{Q}(t) - \dot{W}(t) + \dot{Q}_{\text{chem}}(t) - \sum_i I_{0i} \dot{N}_{i1}(t), \quad (8)$$

where  $\dot{Q}$  is the rate at which heat is transferred into the bubble,  $\dot{W}$  is the rate at which work is done by the bubble,  $\dot{Q}_{\text{chem}}$  is the rate at which the internal energy changes due to chemical reactions;  $I_{0i}$  is the (reduced) ionization potential of species  $i$ , and  $\dot{N}_{i1}$  is the rate at which singly ionized ions of species  $i$  are produced. The internal energy of the bubble is given by the translational, rotational, and vibrational degrees of freedom  $f_i$  of the atoms and molecules in the bubble, and the translational energy of the electrons  $N_e$ ,

$$E(t) = \left( \sum_i \frac{f_i [T(t)]}{2} N_i(t) + \frac{3}{2} N_e(t) \right) k_B T(t). \quad (9)$$

All particles possess three translational degrees of freedom; diatomic molecules have two and nonlinear polyatomic molecules have three additional rotational degrees of freedom. We also include the vibrational degrees of freedom of the molecules  $\text{H}_2\text{O}$ ,  $\text{OH}$ ,  $\text{O}_2$ , and  $\text{H}_2$ , but not of  $\text{HO}_2$ ,  $\text{O}_3$ , and  $\text{H}_2\text{O}_2$ , since these are present only in small amounts. The populations of the vibrational excitations for molecule  $i$  as a function of temperature is given by

$$f_i^{\text{vib}}(T) = 2 \sum_{j=1}^{j_{\text{max}}} \frac{\theta_{ij}/T}{e^{\theta_{ij}/T} - 1}, \quad (10)$$

where the factor 2 accounts for the potential energy associated with the kinetic energy of vibration. The  $\theta_{ij}$  are the

characteristic vibrational temperatures for the given molecule  $i$  [23];  $j_{\max}=3$  for water,  $j_{\max}=1$  for the diatomic gases.

The heat transfer into the bubble may be described according to [11]

$$\dot{Q}(t) = 4\pi R(t)^2 \kappa_{\text{H}_2\text{O}}(T_\infty) \frac{T_\infty - T(t)}{a\ell(t)}, \quad (11)$$

where we use, comparable with Ref. [11],  $a=2.5$ ;  $\kappa_{\text{H}_2\text{O}}$  is the coefficient of heat conduction of water vapor and we estimate the mean free path  $\ell$  of water molecules in the gas by

$$\ell(t) = \frac{1}{\sqrt{2}\sigma_{\text{H}_2\text{O}}n_{\text{tot}}^s(t)}. \quad (12)$$

We take the cross section of a water molecule to be  $\sigma_{\text{H}_2\text{O}} = 2.2 \times 10^{-19} \text{ m}^2$  and the number density  $n_{\text{tot}}^s(t) = n_{\text{H}_2\text{O}}^s(t) + n_X(t)$ ;  $n_X(t) = N_X/V(t)$  where  $N_X$  is the number of rare-gas atoms of type  $X$  in the bubble and  $n_{\text{H}_2\text{O}}^s = p_{\text{H}_2\text{O}}^{\text{vap}}(T_\infty)/k_B T_\infty$ . The rate of work done by the bubble against the external pressure  $p$  is given by

$$\dot{W}(t) = p(t)\dot{V}(t). \quad (13)$$

Finally, the bubble will gain energy  $Q_{\text{chem}}$  through the enthalpy changes associated with the chemical reactions

$$\dot{Q}_{\text{chem}}(t) = \sum_\gamma [R_\gamma^b(t) - R_\gamma^f(t)] \Delta H_\gamma^f, \quad (14)$$

where  $R_\gamma^f(t)$  and  $R_\gamma^b(t)$  are the forward and backward rates of chemical reaction  $\gamma$  and  $\Delta H_\gamma^f$  is the enthalpy change per forward reaction. We note that  $\Delta H_\gamma^f < 0$  if reaction  $\gamma$  is exothermic in forward direction and ‘‘forward direction’’ means reaction from left to right in Eq. (18) below.

The rate of change of the internal bubble energy, Eq. (8), as a function of the varying temperature, is given by

$$\dot{E} = \frac{dE}{dt} = C_v \dot{T} + \sum_i \frac{\partial E}{\partial N_i} \dot{N}_i, \quad (15)$$

where  $C_v$  is the specific heat at constant volume. The total variation of the temperature is thus given by

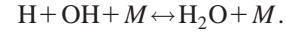
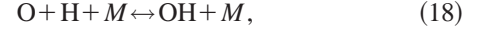
$$\begin{aligned} \dot{T}(t) = & \frac{\dot{Q}(t)}{C_v(t)} - \frac{p(t)\dot{V}(t)}{C_v(t)} + \frac{8}{2} k_B T_\infty \dot{N}_{\text{H}_2\text{O}}^{\text{wall}}(t) \\ & - \sum_i \frac{f_i[T(t)]}{2} \frac{\dot{N}_i(t) k_B T(t)}{C_v(t)} \\ & + \frac{\dot{Q}_{\text{chem}}(t)}{C_v(t)} - \sum_i \frac{I_{0i} \dot{N}_{1i}(t)}{C_v(t)}, \end{aligned} \quad (16)$$

with

$$\begin{aligned} C_v(t) = & \frac{3}{2} N_e k_B + \sum_i \left( \frac{f_i[T(t)]}{2} N_i(t) k_B \right. \\ & \left. + \frac{1}{2} \frac{df_i[T(t)]}{dT(t)} N_i(t) k_B T(t) \right). \end{aligned} \quad (17)$$

### III. CHEMISTRY

Water molecules dissociate as the bubble is compressed and heats up. We account for a number of reactions of  $\text{H}_2\text{O}$  and eight derivatives ( $\text{OH}$ ,  $\text{O}_2$ ,  $\text{H}_2$ ,  $\text{O}$ ,  $\text{H}$ ,  $\text{O}_3$ ,  $\text{HO}_2$ ,  $\text{H}_2\text{O}_2$ ), as well as the rare gas  $X$ ; the most important ones being



Here  $M$  represents a nonreactive participant of a reaction, which can be any atom or molecule present in the bubble. Twenty-three other reactions are not listed here for simplicity, but are nevertheless included in our calculations. All reactions and their thermodynamic parameters as used here are taken from Table I of Ref. [11]; see also Ref. [20].

The forward/backward rate  $r_\gamma^{f/b}$  ( $R_\gamma^{f/b} = V r_\gamma^{f/b}$ ) of a chemical reaction  $\gamma$  is given by

$$r_\gamma^{f/b} = k_\gamma^{f/b} \prod_j n_j, \quad (19)$$

where the  $n_j = N_j/V$  are number densities of species  $j$ , the product is over all species  $j$  participating in the reaction  $\gamma$  and  $k_\gamma^{f/b}$  is given by an empirical Arrhenius-type equation

$$k_\gamma^{f/b} = A_\gamma^{f/b} T^{\beta_\gamma^{f/b}} \exp(-C_\gamma^{f/b}/T). \quad (20)$$

Here the thermodynamic parameters of the reactions are  $C_\gamma^{f/b}$  (in K) and  $A_\gamma^{f/b}$  in  $\text{m}^3/(\text{s K}^{\beta_\gamma^{f/b}})$  for a two-body reaction and in  $\text{m}^6/(\text{s K}^{\beta_\gamma^{f/b}})$  for a three-body reaction. The  $A_\gamma^{f/b}$  is taken from Ref. [11], divided by Avogadro’s number,  $N_a$  for two- and the square  $N_a^2$  for three-body reactions.

The change of the number of species  $i$  is then given by the rates of reactions that generate or destroy that species,  $r_{ji}^g$  and  $r_{ki}^d$ , respectively, according to

$$\dot{N}_i = V \left( \sum_j r_{ji}^g - \sum_k r_{ki}^d \right), \quad (21)$$

where the  $r_\gamma^{f/b}$ , Eq. (19), have to be substituted for the  $r_{ji}^g$  or  $r_{ki}^d$  as appropriate.

### IV. IONIZATION

The degree of ionization of the gas mixture in the bubble is calculated in two ways, (i) from a multicomponent Saha equation [24] and (ii) from ionization and recombination rate equations [25,26]. In the first case thermal equilibrium is assumed. The second calculation serves as a test of this assumption and permits the calculation of the ionization rates

required for the determination of the energy loss due to ionization, the last term of Eqs. (8) or (16).

### A. Partition functions

Ionization equilibria and rates are computed from the partition functions  $Z_{ji}(T)$  of ionization stage  $j$  of species  $i$

$$\begin{aligned} Z_{ji}(T) &= \sum_k g_{kji} \exp\left(-\frac{I_{kji}}{k_B T}\right) \\ &= g_{0ji} + g_{1ji} \exp\left(-\frac{I_{1ji}}{k_B T}\right) + \dots, \end{aligned} \quad (22)$$

where the sum extends over all excitation levels  $k$  of ionization stage  $j$  of species  $i$  with statistical weight  $g_{kji}$  and ionization energy  $I_{kji}$ . Here the energies in the partition functions are normalized such that the ground-state energy of each ionization stage is  $I_{0ji}=0$ , while the energy difference between the ground-state levels of ionization stage  $j$  and  $j+1$  is given by the ionization potential  $I_{ji}$  of ionization stage  $j$ . That is why  $I_{ji}$  appears below, Eq. (30), explicitly.

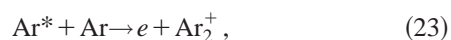
The partition functions of the monatomic gases are calculated from the atomic energy levels and their statistical weights [27]. All energy levels below 10 eV are taken into account. For ionized xenon, we used the fit of the partition function given in Ref. [28] to extract energy levels, assuming a level structure similar to that of the other rare gases.

Partition functions of diatomic molecules are more complex since rovibrational levels have to be taken into account. We use analytical approximations that are valid from 1000 K to 9000 K [29]; above 9000 K we use the result obtained for 9000 K. At such high temperatures the number of diatomic molecules in the bubble is negligible so that no large errors arise. This was confirmed by simple numerical tests.

For molecules with more than two atoms we set all partition functions equal to 1, since only ratios of partition functions enter Eq. (30). Again, at temperatures when ionization occurs, the concentrations of polyatomic molecules are very small.

### B. Reduction of ionization potential

In dense fluids ionization potentials are lowered by several mechanisms. For example, the higher-lying electronic states of the atoms tend to get blurred and the effective ionization potential lowered, the more so the higher the density [30–35]. Electronic levels tend to form bandlike structures and the effective ionization potential may become the low-energy limit of the conduction band. A whole range of high-lying excited states is thus removed at liquid densities [36]. Moreover, when ionization by electron impact occurs, electronic states of rare-gas atoms with excitation energies of a few eV below ionization are also excited. Some of these excited atom states react immediately with ground-state atoms, e.g.,



creating an electron-ion pair by associative ionization [36,37] (Hornbeck-Molnar reaction). For these types of ionizations an effective ionization potential must be used in Eq. (30) below, which is lower than the well-known atomic ionization potentials by about 1 eV. We note that, in the case of argon, associative ionization was shown to contribute to the reduction of the ionization potential at the triple point [36], but associative ionization is known to occur in all rare gases, even at much lower densities than are of interest here.

In *plasmas*, the Debye theory [31] gives a lowering of the ionization potentials according to

$$\Delta I_D(n_e, T) = \frac{e^2}{4\pi\epsilon_0\rho_D(n_e, T)}, \quad (24)$$

where the Debye radius  $\rho_D(n_e, T)$  is a function of the electron density and temperature,

$$\rho_D(n_e, T) = \sqrt{\frac{\epsilon_0 k_B T}{2e^2 n_e}}, \quad (25)$$

where  $e$  is the charge of the electron and  $\epsilon_0$  is the dielectric constant of vacuum. For very large electron densities  $n_e$  it is, however, more appropriate to use the reduction given by the ion-sphere model [31,38]

$$\Delta I_{IS}(n_e) = \frac{3}{4} \frac{e^2}{4\pi\epsilon_0 R_0(n_e)}, \quad (26)$$

with  $R_0$  given by

$$\frac{4\pi}{3} R_0^3 n_e = 1. \quad (27)$$

Summarizing, to account for the plasma effects, we use a reduction of the ionization potential [31]

$$\Delta I_{\text{Ion}}(n_e, T) = \min(\Delta I_D(n_e, T), \Delta I_{IS}(n_e)). \quad (28)$$

To also take associative ionization processes, Eq. (23), into account, for the rare gases we use

$$\Delta I(n_e, T) = \max(\Delta I_{\text{Ion}}(n_e, T), \Delta I_{\text{HM}}), \quad (29)$$

where  $\Delta I_{\text{HM}}$  is the effective reduction due to associative ionization, Eq. (23). For xenon we use  $\Delta I_{\text{HM}}=1.02$  eV [35], for argon  $\Delta I_{\text{HM}}=1.23$  eV [36], and for helium  $\Delta I_{\text{HM}}=1.4$  eV [37]. The maximum reduction of the ionization potential due to high electron and high neutral densities is of roughly the same magnitude.

### C. Saha equation

Assuming local thermal equilibrium, the number density  $n_{ji}$  of atoms (molecules) of species  $i$  in ionization stage  $j$  is given by [24]

$$\begin{aligned} \frac{n_{ji}}{n_{j+1,i}} &= n_e \frac{Z_{ji}(T)}{Z_{j+1,i}(T)} \frac{1}{2} \left( \frac{h^2}{2\pi m_e k_B T} \right)^{3/2} \exp\left(-\frac{I_{ji}}{k_B T}\right) \\ &\equiv n_e \Phi_{ji}(T). \end{aligned} \quad (30)$$

Here,  $n_e$  is the electron number density,  $h$  is Planck's constant,  $m_e$  the electron mass,  $T$  the temperature,  $I_{ji}$  the ionization energy of the  $j$ th ionization stage of species  $i$  (i.e., it is the energy necessary to remove the  $(j+1)$ -th electron from the atom), and  $Z_{ji}(T)$  its partition function, Eq. (22). For the ionization energy we use the tabulated low density value reduced by the value determined above, Eq. (29).

From Eq. (30), the density  $n_{ji}$  is given by

$$n_{ji} = n_{J_i} \frac{n_{J_i-1,i}}{n_{J_i}} \cdots \frac{n_{ji}}{n_{j+1,i}} = n_{J_i} \prod_{l=j}^{J_i-1} [n_e \Phi_{li}(T)], \quad (31)$$

where  $J_i$  is the highest ionization stage considered for species  $i$ . Thus, for species  $i$  the total number density  $n_i$  of particles is

$$n_i = \sum_{m=0}^{J_i} n_{mi} \quad (32)$$

and the fraction  $f_{ji}(n_e, T)$  of the number density of particles of type  $i$  in ionization stage  $j$  relative to the total number density of particles of type  $i$  is then given by

$$f_{ji}(n_e, T) = \frac{n_{ji}}{n_i} = \frac{\prod_{l=j}^{J_i-1} [n_e \Phi_{li}(T)]}{\sum_{m=0}^{J_i} \prod_{l=m}^{J_i-1} [n_e \Phi_{li}(T)]}. \quad (33)$$

The condition of the overall neutrality of the bubble interior is

$$n_e = \sum_i \sum_{j=1}^{J_i} j n_{ji} = \sum_i n_i \sum_{j=1}^{J_i} j f_{ji}(n_e, T) \equiv \Theta(n_e, T). \quad (34)$$

We solve Eq. (34) for  $n_e$  by an iterative procedure. Assume we have an estimate  $n_e^0$  for  $n_e$ , such that  $n_e = n_e^0 + \delta n_e$  with  $\delta n_e$  small. Since Eq. (34) is nonlinear, we cannot determine  $\delta n_e$  exactly, but we can estimate it by expanding all terms to first order in  $\delta n_e$ , i.e.,  $f(n_e) \approx f(n_e^0) + [\partial f(n_e)/\partial n_e]_{n_e^0} \delta n_e$ :

$$n_e^0 + \delta n_e \approx \Theta(n_e^0, T) + \left[ \frac{\partial \Theta(n_e, T)}{\partial n_e} \right]_{n_e^0} \delta n_e \quad (35)$$

and thus

$$\delta n_e \approx \frac{\Theta(n_e^0, T) - n_e^0}{1 - \left[ \frac{\partial \Theta(n_e, T)}{\partial n_e} \right]_{n_e^0}}. \quad (36)$$

If only the first ionization stage is included in the calculation, the degree of ionization of species  $i$ , i.e., the fraction of atoms or molecules of  $i$  that are singly ionized, is finally given by

$$f_{1i}(n_e, T) = \frac{1}{1 + n_e \Phi_{0i}(n_e, T)}, \quad (37)$$

see Eq. (33).

#### D. Ionization rates

We also compute the degree of ionization of the bubble gas using rate equations, which is, however, more computationally intensive since in that case we have to solve 22 instead of 12 simultaneous differential equations. The only processes we consider explicitly through rate equations are electron impact ionization (or collisional ionization) and its inverse process, three-body recombination, with rates  $\alpha_{i,0 \rightarrow 1}^{\text{ion}}$  and  $\alpha_{i,1 \rightarrow 0}^{\text{rec}}$ , respectively. Implicitly, through the reduced ionization potential, we also include associative ionization and its inverse process, dissociative recombination. We neglect negative-positive ion recombination because of the small number of negative ions present. Also photoionization and radiative recombination are neglected here (but of course not as light emitting mechanisms) because of the small number of photons present, relative to the number of electrons. The change in number density of species  $i$  in ionization stage 0 is then given by

$$\dot{n}_{0i} = -n_{0i} n_e \alpha_{i,0 \rightarrow 1}^{\text{ion}} + n_{1i} n_e \alpha_{i,1 \rightarrow 0}^{\text{rec}} \quad (38)$$

and, since we again only include single ionization, the change in number density of species  $i$  in ionization stage 1 is

$$\dot{n}_{1i} = -\dot{n}_{0i}. \quad (39)$$

The rate for electron impact ionization of each species  $i$  is given by [25,26]

$$\alpha_{i,0 \rightarrow 1}^{\text{ion}} = 1.86 \times 10^{-13} T^{1/2} \exp(-I_{0i}/k_B T) \times [1 - \exp(-I_{0i}/k_B T)] \left( \frac{I_{0H}}{I_{0i}} \right)^2 \mathcal{G}, \quad (40)$$

where  $I_{0H}$  is the ionization potential of hydrogen and  $\mathcal{G}$  is the Gaunt factor. We currently simply set  $\mathcal{G}=1$ , but its choice does not really matter as will be seen below.

In thermal equilibrium, i.e., if  $\dot{n}_{1i} = -\dot{n}_{0i} = 0$  in Eq. (38), from the rate equations the same degree of ionization must be obtained as from the Saha equation. Thus with Eq. (30) the rate of three-body recombination must be given by

$$\alpha_{i,1 \rightarrow 0}^{\text{rec}} = n_e \Phi_{0i}(n_e, T) \alpha_{i,0 \rightarrow 1}^{\text{ion}}. \quad (41)$$

#### V. LIGHT EMITTING PROCESSES

As in previous sonoluminescence models [12,13,15] the light emitting processes considered are bremsstrahlung produced by collisions of electrons with neutral and ionized rare-gas atoms. In addition, we also include here the bremsstrahlung produced by electron collisions with the other atoms and molecules present in the bubble. Furthermore, radiative attachment of electrons to neutral hydrogen and oxygen atoms, and electron-ion radiative recombination are

TABLE I. Wavelengths  $\lambda_{2,i}$  used for the atomic gases in Eq. (43).

Gas	He	Ar	Xe	H	O
$\lambda_{2,i}$ (nm)	260	294	366	364	431

accounted for. We also looked at charge exchange radiation [39] and polarization bremsstrahlung [40–42]. As in previous work [12,15], to account for the small, but non-negligible optical thickness of the sonoluminescent bubble, we calculate absorption coefficients and then use the radiative transfer equation to convert to emission, assuming local thermal equilibrium [12,43].

### A. Electron-neutral bremsstrahlung

Electron-atom bremsstrahlung spectra of the rare-gas atoms are computed with the help of a quantum line shape formalism; details may be found elsewhere [44]. The electron-atom bremsstrahlung spectra of hydrogen and oxygen atoms are computed here in the same manner, using the interaction potential parameters obtained elsewhere [45]. For the neutral molecules containing  $n$  hydrogen atoms and  $m$  oxygen atoms, we estimate the electron-neutral bremsstrahlung contributions from free electrons by adding  $n$  times the radiation of hydrogen atoms plus  $m$  times those of oxygen atoms, but we note that the inclusion or omission of such estimates of molecular contributions did not affect the end results.

### B. Polarization bremsstrahlung

We also consider the mechanism of electron-atom polarization bremsstrahlung, where the neutral atom is polarized in the Coulomb field of the electron in the fly-by encounter; the resulting time-varying dipole moment emits light [40,41]. Under sonoluminescence conditions such contributions were found to amount to less than 10% of the electron-atom bremsstrahlung contributions [42].

### C. Electron-ion bremsstrahlung and recombination radiation

We treat electron-ion bremsstrahlung and recombination radiation separately. The coefficient  $\kappa_i^{ff+}(\lambda)$  describing bremsstrahlung of free electrons interacting with ion species  $i$  is given by [43]

$$\kappa_i^{ff+}(\lambda) = \frac{4}{3} \left( \frac{2\pi}{3m_e k_B T} \right)^{1/2} \frac{e^6}{(4\pi\epsilon_0)^3 m_e h c^4} n_{1i} n_e \lambda^3 \times \left[ 1 - \exp\left(-\frac{hc}{\lambda k_B T}\right) \right]. \quad (42)$$

The coefficient  $\kappa_i^{bf+}(\lambda)$  describing electron-ion recombination radiation of species  $i$  is obtained from a hydrogenlike atom model [43], given by

TABLE II. Parameters used to represent the photodetachment cross section of  $O^-$   $\sigma_{O^-}(\lambda)$ , (as in Eq. (46)).

$i$	$a_i$ ( $10^{-22}m^2$ )	$E_i$ (eV)	$n_i$	$d_i$
1	10.85	1.466	4.0	0.35
2	70.0	3.4	3.8	1.3
3	42.0	5.6	4.5	1.25

$$\kappa_i^{bf+}(\lambda) = \frac{64\pi^4}{3\sqrt{3}} \frac{e^{10}m_e}{(4\pi\epsilon_0)^5 h^6 c^4} \lambda^3 n_{0i} \left[ 1 - \exp\left(-\frac{hc}{\lambda k_B T}\right) \right] \times \left[ \exp\left(\frac{hc/\max\{\lambda, \lambda_{2,i}\}}{k_B T}\right) - 1 \right]. \quad (43)$$

For atomic gases the wavelengths  $\lambda_{2,i}$  correspond to the energy difference between the first excited state and a quasi-continuum of states [12,43]; the  $\lambda_{2,i}$  are given in Table I. For the rare gases and hydrogen, this model is justified [12], but in the case of oxygen atoms, a modification is necessary because of the low excitation energies of the oxygen atom. The value of  $\lambda_{2,i}$  we chose for oxygen represents the wavelength where the continuum model for the higher-lying states can be applied, while disregarding some lower states. But we note that the radiative recombination of oxygen ions  $O^+$  contributes little to the overall emission, see below. For the molecular gases we set  $\lambda_{2,i}=0$  since there are energy levels available for almost any photonic energy; this choice should also give an upper limit of intensity. It turns out that under no circumstances molecular radiation contributes discernibly to the total intensity, see Fig. 1. This is not surprising, since significant emission occurs at temperatures high enough so that virtually all molecules are dissociated.

### D. Radiative attachment

A most efficient process is radiative attachment of electrons to hydrogen [46–48,31] and oxygen atoms [43,49,50]; see also Refs. [51,52,24]. For an assessment of the significance of radiative attachment for sonoluminescence, tabulated absorption cross sections  $\sigma_{H^-}(\lambda)$  of  $H^-$  as function of the photon wavelength, are available [53]. The effective absorption coefficient, corrected for induced emission, is obtained according to

$$\kappa_{H^-}(\lambda) = \sigma_{H^-}(\lambda) n_{H^-} [1 - \exp(-hc/\lambda k_B T)]. \quad (44)$$

The number density of negatively charged hydrogen ions is given by an expression such as Eq. (30),

$$\frac{n_{H^-}}{n_H} = n_e \frac{Z_{H^-}}{Z_H} \frac{1}{2} \left( \frac{h^2}{2\pi m_e k_B T} \right)^{3/2} \exp\left(\frac{I_{H^-}}{k_B T}\right), \quad (45)$$

with  $Z_{H^-}=1$ ,  $Z_H=2$ , and the electron affinity  $I_{H^-}=0.754$  eV. Similarly, for  $O^-$  the absorption cross section  $\sigma_{O^-}(\lambda)$  is given as analytic fit of direct measurements [54],

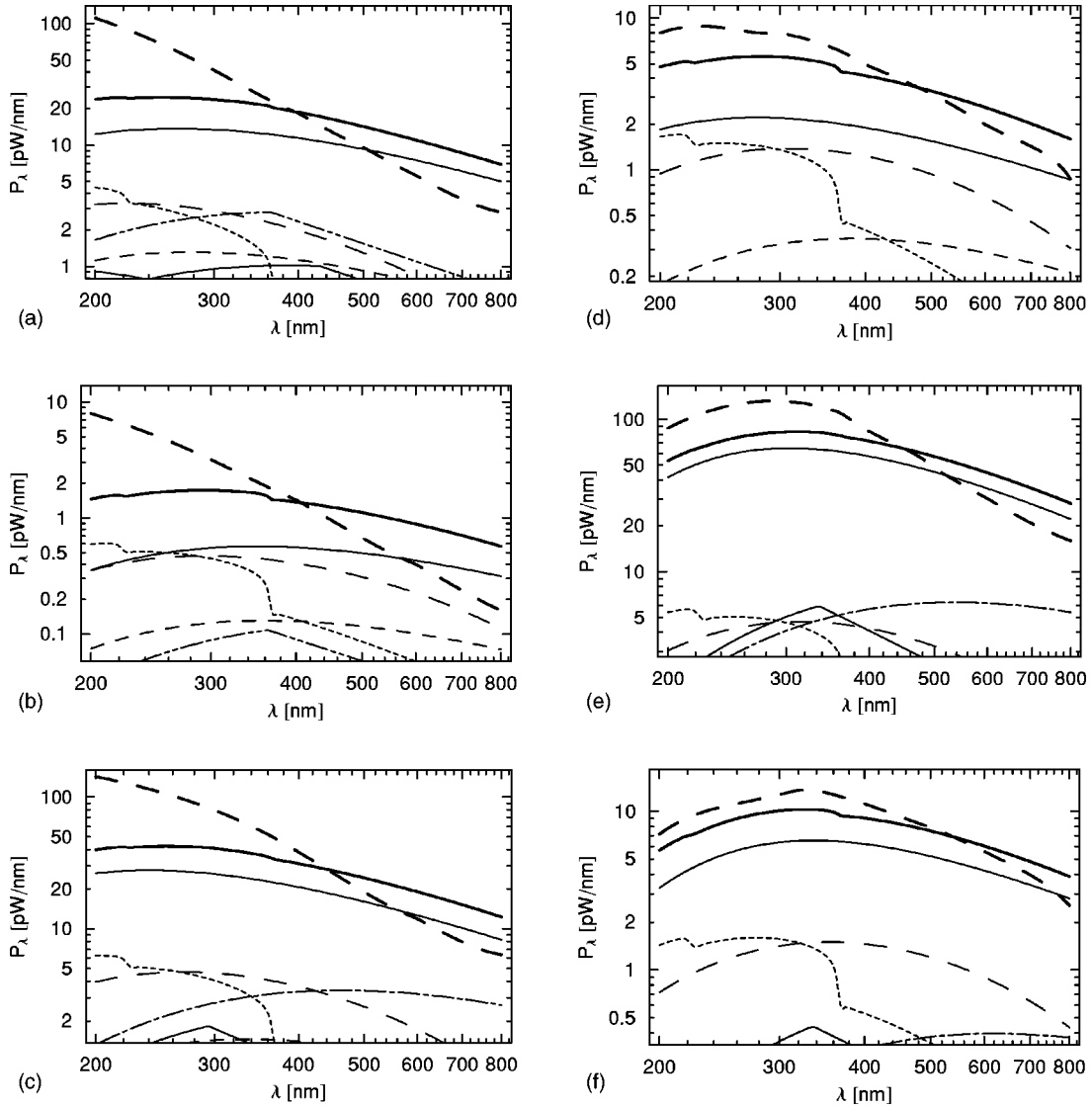


FIG. 1. The spectra and their composition for, from top to bottom, helium, argon, and xenon at freezing water temperature (left panel) and for water at room temperature (right panel). Shown are the computed spectra (thick solid line). Contributions due to electron-neutral rare gas atom bremsstrahlung (thin solid line),  $O^-$  radiation (dotted line),  $H^-$  radiation (long-dashed line),  $e-X^+$  (dash-dotted line),  $e-H^0$  (short-dashed line),  $e-H^+$  (dash-double-dotted line) are also given. Various other mechanisms that contribute weakly are also shown by thin solid lines in the lower parts of the plots. For comparison, experimentally obtained spectra are indicated by the thick dashed lines [7,55].

$$\sigma_{O^-}[E(\lambda)] = \sum_{i=1}^3 a_i \left( \frac{\max\{0, E(\lambda) - E_{ij}\}}{E(\lambda)} \right)^{1/n_i} E(\lambda)^{-d_i}, \quad (46)$$

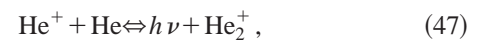
with the photon energy  $E(\lambda) = hc/\lambda$  and the fit parameters shown in Table II. For the partition function of the negative oxygen ions we use  $Z_{O^-} = 6$  and an electron affinity of  $I_{O^-} = 1.465$  eV.

Note that strictly speaking the use of Eq. (45) only in the computation of the absorption coefficient is inconsistent with the scheme described in Secs. IV C and IV D; instead Eq. (45) should be used in the recursive solution of the Saha equation, or with the rate equations. However, it turns out that using Eq. (45) as described here has no significant influence on the total emitted energy.

We neglect molecular negative ions such as  $OH^-$  or  $O_2^-$ , because, again, at the temperatures of interest here virtually all molecules are dissociated.

### E. Charge exchange radiation and related processes

We also considered radiative ion-atom association,



ion-atom bremsstrahlung and charge exchange,

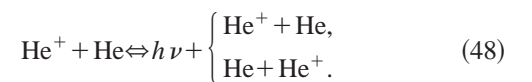


TABLE III. An illustration of the effects on temperature, pulse duration, and photon numbers of accounting for the energy loss due to ionization, electron pressure, and electron heat capacity. The results shown are for an argon bubble at  $T_\infty=20^\circ\text{C}$ ,  $\nu_a=20\text{ kHz}$ ,  $P_a=1.3\text{ bar}$ ,  $R_0=5\ \mu\text{m}$ , but are representative for all cases of interest here. Row *a* shows a calculation where none of the effects are accounted for, for comparison with row *b* where only the energy loss due to ionization was taken into account. For the results of row *c* the effects of the electron pressure and heat capacity are also included.

	$R_{\max}$ ( $\mu\text{m}$ )	$R_{\min}$ ( $\mu\text{m}$ )	$T_{\max}$ (K)	$\Delta t_{\text{Pulse}}$ (ps)	$n_{\text{Phot}}^{\text{calc}}$
<i>a</i>	52.1	0.810	16 020	183	653 000
<i>b</i>	52.1	0.803	15 289	207	489 000
<i>c</i>	52.1	0.804	15 263	206	483 000

Emission and absorption coefficients for these processes are known for helium and some other gases [39]. We generally find these processes, Eqs. (47), (48), to contribute little to the emitted intensity because of the small number of positive helium ions in the bubble. However, the reactions, Eqs. (47), (48), become quite significant when we consider the hotter, nonisotropically heated bubbles, as we will see in Sec. VI F. We note here, however, that in the dense environment of sonoluminescence most likely no  $\text{He}^+$  ions exist. Instead, in nonradiative collisions, and by radiative association, Eq. (47), the atomic ions will quickly form molecular ions,  $\text{He}_2^+$ , etc. Also, molecular ions are formed efficiently directly from excited atoms, Eq. (23). These effects will reduce the significance of ion-atom bremsstrahlung and charge exchange radiation, Eq. (48). On the other hand, the efficiency of radiative ion-atom association, Eq. (47), should be largely unaffected. This process, however, generates most of the light in the blue and ultraviolet parts of the spectrum [39]. This fact will interest us below, Sec. VI F.

## VI. RESULTS

First, we discuss various aspects of computing the degree of ionization. We also illustrate the effects the free electrons have on the bubble dynamics (Table III). We then show more general results of our model calculations concerning bubble dynamics and the widths and intensities of the emitted light pulses, Tables IV to VI. The dependence of these observables on the rare-gas type and the water temperature is illustrated. Figure 1 shows the spectra obtained from the model, along

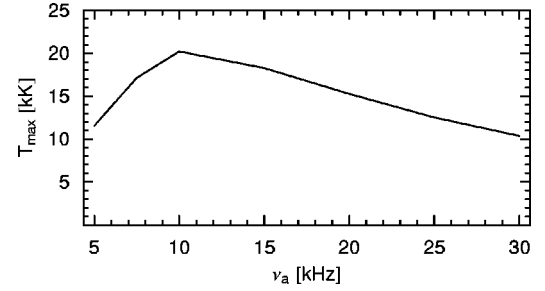


FIG. 2. Maximum temperature of an argon bubble with  $R_0=5\ \mu\text{m}$ ,  $P_a=1.3\text{ bar}$ ,  $T_0=20^\circ\text{C}$  as function of driving frequency. Compare with Fig. 4 of Ref. [17].

with the relative importance of the various radiative processes. We plot the temperature in the bubble as a function of acoustic driving frequency in Fig. 2, as an illustration of the significance of water vapor content at low driving frequencies. Furthermore, we look briefly at the effects of modifying the equation of state and the chemical reaction scheme. Finally we discuss possible modifications of our model, which are necessary to better match computed spectra of helium bubbles to observation.

### A. Ionization

The radiative processes of interest for single bubble sonoluminescence all involve electrons and ions [9]. A careful modeling of the degree of ionization that is consistent with the parameter space of the hydrodynamic model is an essential precondition for a successful modeling of spectral intensities. We therefore study this important link in some detail.

All computations of the degree of ionization require the partition functions, Eq. (22), of the neutral and ionized species. We attempt to improve the treatment of ionization over the hydrogenlike atom model used previously. The resulting differences are substantial. For the rare gases the statistical weight  $g$  of the neutral state is 1 because of the closed electronic shell while for hydrogen it is 2 due to the two different orientations of the spin of the single electron. On the other hand, in the ionized state the statistical weight of hydrogen is 1 since it has lost its only electron while for the rare gases the weight equals 6 (or 2 in the case of helium). In other words, while for hydrogen the neutral state has a larger statistical weight than the ionized state, for the rare gases the opposite is the case. Thus, for the rare gases the ionization balance shifts to the ionized state, thereby increasing the

TABLE IV. Input parameters and hydrodynamic data of the calculations, and comparison with observed photon numbers for water at freezing temperature. All calculations with  $T_\infty=0^\circ\text{C}$ ,  $\nu_a=33.4\text{ kHz}$ ,  $P_0=1.01325\text{ bar}$ ,  $R_0=5.5\ \mu\text{m}$ .

Gas	$P_a$ (bar)	$R_{\max}$ ( $\mu\text{m}$ )	$p_{\text{H}_2\text{O}}^m$ (%)	$\dot{R}_{\max}$ (m/s)	$R_{\min}$ ( $\mu\text{m}$ )	$T_{\max}$ (K)	$p_X^m$ (%)	$\Delta t_{\text{Pulse}}$ (ps)	$n_{\text{Phot}}^{\text{calc}}$	$n_{\text{Phot}}^{\text{obs}}$
He	1.53	52.2	95.1	-1336	0.888	19 997	90.4	254	599 000	625 000
Ar	1.48	48.3	60.0	-1175	0.915	16 112	99.2	270	1 034 000	1 181 000
Xe	1.45	45.9	28.2	-1046	0.985	13 756	99.8	324	2 289 000	2 227 000

TABLE V. Input parameters and hydrodynamic data of the calculations, and comparison with observed photon numbers for water at room temperature. All calculations with  $T_\infty=20$  °C,  $\nu_a=33.4$  kHz,  $P_0=1.013\,25$  bar,  $R_0=4.5$   $\mu\text{m}$ .

Gas	$P_a$ (bar)	$R_{\max}$ ( $\mu\text{m}$ )	$p_{\text{H}_2\text{O}}^m$ (%)	$\dot{R}_{\max}$ (m/s)	$R_{\min}$ ( $\mu\text{m}$ )	$T_{\max}$ (K)	$p_X^m$ (%)	$\Delta t_{\text{Pulse}}$ (ps)	$n_{\text{Phot}}^{\text{calc}}$	$n_{\text{Phot}}^{\text{obs}}$
He	1.40	41.2	98.5	-1259	0.702	15 060	82.8	179	46 000	46 000
Ar	1.39	40.3	85.1	-1192	0.731	14 048	98.1	186	138 000	143 000
Xe	1.36	37.8	58.9	-1028	0.791	12 053	99.5	218	297 000	308 000

photon yield. The intensity of all light emitting mechanisms considered in this paper is proportional to at least the first power of the degree of ionization. For example, in the test case of an argon bubble with the parameters as given in the caption of Table III the difference was roughly a factor 2.5 in the number of emitted photons. Furthermore, accounting for the reduction of the ionization potential, Sec. IV B, increases the light output additionally by about 50%.

Next we confirmed that the degrees of ionization calculated from the Saha equation and from the rate equations agree closely. One may therefore say that thermal equilibrium with respect to ionization is reached in our calculations. This is the case largely regardless of the value chosen for the Gaunt factor  $\mathcal{G}$ , Eq. (40): speeding up ionization by increasing  $\mathcal{G}$  also speeds up recombination and thus equilibrium is established even faster. On the other hand, even with  $\mathcal{G}=0.1$  we still obtain a result equal to that using the Saha equation. It may thus seem that elaborate rate equations to compute the ionization in the bubble may be dispensed with, since the much simpler Saha equation approach gives the same result.

However, to assess the significance of energy losses of the bubble due to the ionization reactions we still need to use rate equations since otherwise the necessary energy loss rates cannot be obtained. This energy loss turns out to be an important effect. The ionization potential of most species in the bubble is around 10 eV. Thus, each ionization reaction consumes a substantial amount of energy, similar to the chemical reactions, see Sec. III. The inclusion of the energy loss due to ionization [the last term of Eqs. (8) or (16)] reduces the maximum bubble temperature in the case shown, rows  $a$  and  $b$  of Table III, by about 700 K. This in turn substantially lowers the calculated number of emitted photons  $n_{\text{Phot}}^{\text{calc}}$ . In computations where the internal temperature is even higher than in the given example (e.g., when the amplitude of the driving pressure is increased) so that a higher degree of ion-

ization is reached this effect will be even bigger; in bubbles with a smaller degree of ionization it will be smaller. On the other hand, including the effect of the free electrons  $N_e$  on the internal pressure [Eq. (2)] and the heat capacity [Eq. (17)] has only a very small influence, as is seen by comparing rows  $b$  and  $c$  of Table III.

We also calculated the light emission including the second ionization stage in some test cases, but found the effects to be negligible. That is not surprising since the energy difference between the singly and doubly ionized state exceeds 10 eV for all gases, thus the ratio of gas in the doubly vs singly ionized state at  $20\,000\text{ K} \approx 2\text{ eV}$  is small, about  $\exp(-10\text{ eV}/2\text{ eV}) \approx 7 \times 10^{-3}$ .

### B. Hydrodynamics and photon numbers

Tables IV and V show details of our simulations for comparison with experiment [7,55]. Since we want to compare our computations with the existing observations, especially with respect to the light emission, we use the spectra recorded in Ref. [7] for all rare gases in water at freezing and room temperature as our benchmark experiment. In these experiments the rare-gas concentration in the water was 3 Torr and the acoustic frequency 33.4 kHz. Unfortunately, however, neither the pressure amplitudes nor the ambient bubble radii were recorded. All we know is that in these experiments the light output was maximized. Thus, we may use bubble stability calculations to estimate the missing input parameters. The largest ambient radius at which bubbles are still stable under the given conditions is roughly 5.5  $\mu\text{m}$  for water at freezing temperature and 4.5  $\mu\text{m}$  for water at room temperature [15]. The corresponding maximum pressure amplitudes follow from diffusive equilibrium calculations and are around 1.5 bar for water at freezing temperature and 1.4 bar for water at room temperature. Thus we choose in each case the input parameters of our computation, the equilib-

TABLE VI. Number of emitted photons at an acoustic driving frequency of 26.5 kHz for argon. The values of the ambient radius  $R_0$  are chosen as in Ref. [60],  $T_\infty$  and  $P_a$  are chosen in agreement with the description of the experiment in Ref. [59], where observed photon numbers are also reported.

$T_\infty$ (°C)	$P_a$ (bar)	$R_0$ ( $\mu\text{m}$ )	$R_{\min}$ ( $\mu\text{m}$ )	$T_{\max}$ (K)	$\Delta t_{\text{Pulse}}$ (ps)	$n_{\text{Phot}}^{\text{calc}}$	$n_{\text{Phot}}^{\text{obs}}$
2.5	1.45	5.0	0.826	19 209	270	3 921 000	4 500 000
20	1.37	4.0	0.655	16 707	174	545 000	550 000
33	1.27	3.5	0.566	12 133	110	16 000	14 000

rium bubble radius  $R_0$  and the acoustic pressure amplitude  $P_a$ , close to these values. The exact values for all input parameters we used are given in Tables IV and V. Also reported in these tables are the results of our calculations.

First we look at the results of the hydrodynamic part of the simulation, the maximum bubble radius  $R_{\max}$ , the relative mass density of water  $p_{\text{H}_2\text{O}}^m$  at the maximum bubble radius, the maximum collapse velocity  $\dot{R}_{\max}$ , the minimum bubble radius  $R_{\min}$ , and the relative mass density of the rare gas  $p_X^m$  at minimum radius.

The values of the maximum bubble radius are in the range typically observed. However, we note that the maximum collapse velocity here is somewhat smaller than in calculations where the first order correction in the Mach number  $\dot{R}/c_l$  in the Rayleigh-Plesset equation, Eq. (1), is neglected. Since these corrections account for energy used to compress the liquid, the reduction of the maximum collapse velocity is not surprising. The minimum bubble radius  $R_{\min}$  reported here is, in turn, comparatively large. Our calculations suggest a compression ratio  $R_{\min}/R_0$  of only about 1:5.6 (Xe) to 1:6.4 (He). This in turn means that the density in the bubble is relatively low, only about 200 to 300 amagat — even when we take into account that the values of the equilibrium bubble radius,  $R_0$ , given above do not include any water vapor, while at  $R_{\min}$  a certain part of the number density is made up of the dissociation products of  $\text{H}_2\text{O}$ . We note that a compression to the van der Waals excluded volume would imply a density of 434 amagat for a pure xenon bubble, 674 amagat for a pure argon bubble, and 945 amagat for a pure helium bubble. The amount of trapped water vapor at minimum radius,  $p_X^m$ , is in our simulations somewhat smaller than reported in Refs. [56,17], but comparable to that of Ref. [11]. As in Ref. [11] we assume that the exchange of water molecules between the liquid and the bubble is limited by evaporation and condensation of water molecules at the bubble surface rather than by diffusion as in Refs. [56,17], see Eq. (5). If the exchange is assumed to be diffusion limited, in the fast collapse phase fewer water molecules reach the bubble surface to exit the bubble, compared to the case where the exchange is limited by the probability of water molecules sticking to the bubble surface. Note that the amount of water in the bubble at maximum radius,  $p_{\text{H}_2\text{O}}^m$ , does not depend very sensitively on the model of the water exchange chosen.

As mentioned above, the amount of water molecules in the bubble during the time of quasiadiabatic heating is rather small in our computations. The dissociation of those few molecules does not consume much energy so that temperatures are reached to match the calculated  $n_{\text{Phot}}^{\text{calc}}$  and observed photon numbers  $n_{\text{Phot}}^{\text{obs}}$  in all cases, even for helium bubbles—something the model without water vapor was unable to do [12], see below, Sec. VI C. Note that we obtained the observed photon numbers shown in Tables IV and V by numerically integrating the measured spectra [7] and applying a correction for an experimental miscalibration [55]. In Tables IV and V we also present the computed pulse widths  $\Delta t_{\text{Pulse}}$ . Unfortunately, pulse widths were not measured in those experiments [7], but our calculated pulse widths are in

the range typically observed in comparable experiments with bright bubbles [57,58]. Moreover, the observed trends [58] that the maximum pulse widths increase from helium to argon to xenon, and that the pulse lengths in cold water are longer than in water at room temperature, are clearly reproduced from theory.

Since the input parameters and photon numbers in Tables IV and V are indirectly derived, in Table VI we compare with another experiment [59] where these data were directly measured. Again the observed light output was maximized for argon bubbles at three different water temperatures. The main reason for the increased light output at lower water temperatures is the increased bubble stability towards larger driving pressure amplitudes [60]. In our comparison with the experiment we use comparable input values as in Refs. [59,60] (see Table VI for details). Agreement of our results with the observations is obtained.

### C. Spectra and contributions of the various radiative processes

Figure 1 shows the spectra corresponding to the data recorded in Tables IV and V, along with the contributions from the various radiative processes discussed above. The experimentally observed spectra [7,55] are also shown.

The spectra feature a broad maximum in the blue or ultraviolet. In some cases weak structures near 370 nm due to the  $\text{O}^-$  radiative attachment are discernible in the calculated profiles. Computed spectra for water at freezing temperature are an order of magnitude more intense than the comparable spectra computed for room temperature, a fact that is also reflected in the number of emitted photons, Tables IV and V.

The most significant emission mechanism is bremsstrahlung from electron–rare-gas-atom collisions, as could be expected from the small degree of ionization, at most a few percent, of the bubble content. However, in the helium and argon bubbles calculated for water at room temperature radiative attachment to  $\text{H}^-$  and  $\text{O}^-$  is of comparable importance. In the other cases, these two processes are among the second most important ones, along with electron-ion and electron-H atom bremsstrahlung.

In the spectra calculated for water at room temperature the electron–rare-gas-ion bremsstrahlung is almost negligible. In these cases the calculated peak temperatures are lower than at near freezing temperatures, see Tables IV and V. At the low peak temperatures few rare-gas atoms are ionized so that electrons are much more likely to collide with a neutral atom. This is especially true for helium bubbles because of the high ionization potential of He. In helium bubbles ionization of species other than He atoms prevails. This fact helps to explain why the present model reproduces the emitted intensities of helium bubbles while a model neglecting the water vapor content of the bubble could not [12]. We note, however, that the relative contributions of the different radiative mechanisms depend especially on the bubble temperatures and its chemical composition and thus also to some degree on the assumptions made in the hydrodynamic part of our simulation.

At the lower water temperatures (0 °C), the experiments and the present simulations both show spectral maxima shifted to shorter wavelengths compared to the room temperature spectra. Similarly, the maxima of the helium profiles appear at shorter wavelengths than those of the argon profiles, which in turn are at shorter wavelengths than those of xenon. (Actually, the measured helium spectra show no maximum in the optical window of water, which suggests that the intensities peak at wavelengths below 200 nm.) In the cases of the argon and xenon bubble at room temperature, the computed spectral profiles agree well with the observations, even when some of the (minor) structures due to radiative attachment of electrons to oxygen atoms are not discernible in the measurements. However, the spectra computed for the rare-gas bubbles in freezing water, especially in the case of helium, lack intensity in the ultraviolet and show excess emission in the red. This disagreement of theory and observation is larger than the estimated uncertainties, about 30%, of the emission coefficients that have entered our computations. We will consider that fact in Sec. VI F.

#### D. Low driving frequency

Using a model that neglects the water vapor in the sonoluminescent bubble [16,61,12] it was predicted that at driving frequencies  $\nu_a$  below 10 kHz the light emission could be increased dramatically [16]: At the lower driving frequency the bubble has more time to expand which in turn causes a more dramatic collapse [16]. However, the subsequent experiment showed that this prediction was incorrect [17], apparently due to the neglect of water vapor. Water vapor reduces the peak temperatures in the bubble because of the energy consumed by the endothermic dissociation reactions. In addition, a less efficient quasiadiabatic heating of the bubble due to the small ratio of specific heats  $c_p/c_v$  of water vapor contributes.

Since we account somewhat differently for the water vapor than in Ref. [17], we also tested our model at low driving frequencies. First we repeated the calculations corresponding to Fig. 4 of Ref. [17], where the peak temperature  $T_{\max}$  in the bubble is shown to be almost independent of the driving frequency  $\nu_a$ . Our result is given in Fig. 2, which also shows that the maximum bubble temperature is limited when the driving frequency is decreased. However, in our computation the temperature as function of acoustic frequency exhibits a slight maximum near 10 kHz. In this frequency range the effect of the more violent compression due to decreasing driving frequency prevails. Yet, for even lower frequency the amount of water vapor trapped in the bubble increases so rapidly that it offsets this effect. At the higher driving frequencies,  $>10$  kHz, at minimum radius roughly 98% of the bubble content is argon. At 10 kHz the argon content still amounts to 90%. However, at 5 kHz the argon content is reduced to about 60%. Note that our model contains one additional process that limits the maximal temperatures, the energy loss due to ionization. For example, our calculation at 7.5 kHz in Fig. 2 gives a temperature of 17 100 K if energy loss due to ionization is accounted for, and 18 000 K if it is not.

For a direct comparison of the emitted light to observation we use input values as given in the description of the experiment [17] and in Ref. [16]:  $\nu_a=7.1$  kHz,  $T_\infty=22$  °C,  $R_0=3.5$   $\mu\text{m}$ ,  $P_a=1.15$  bar. With  $a=2$  [Eq. (11)] we obtain a photon yield of  $3\times 10^4$  photons and a pulse width of 103 ps, both in reasonable agreement with the measurement [17].

#### E. Equation of state and chemistry

We considered several minor modifications of the equation of state, Eq. (2). For example, including the internal pressure term  $a_i/V^2$  in the van der Waals equation has a negligible effect, as might be expected. In the test cases studied, the peak temperature in the bubble changed by less than about 200 K out of more than 10 000 K.

Conceivably more important might be the temperature dependence of the excluded volume  $b_i$ , Eq. (2), that is commonly neglected. In the hard sphere approximation, the excluded volume  $b_i$  is constant, but at higher temperatures real atoms and molecules appear somewhat smaller than at lower temperatures as realistic interaction potentials suggest [62]. Realistic  $b_i$  parameters should therefore decrease slightly with increasing temperature. In order to investigate the significance of this temperature dependence, we estimated a temperature-dependent second virial coefficient from an accurate Ar-Ar interaction potential [63]. The excluded volume  $b_i$  equals the second virial coefficient when Eq. (2) is expanded in a virial series. However, the comparison of simulations based on such a refined model of the excluded volume  $b(T)$  with the more conventional models that neglect the temperature dependence suggests peak temperatures that differ by an insignificant amount of about 200 K. On the other hand, comparing a calculation using the full van der Waals equation with a calculation employing the truncated virial expansion shows a difference of about 1000 K. At the enormous densities at the point of maximum compression a virial expansion of the equation of state, truncated to second order, can hardly be expected to be of sufficient accuracy [62,64].

Finally, we looked at the chemical reaction scheme, as indicated by Eq. (18). It turns out that the reactions involving  $\text{O}_3$  can be safely neglected since doing so changed the peak temperature by less than 100 K. The other species, however, do matter. When ignoring all of them except for the direct dissociation products of water (OH, O, H), the peak temperature rises by about 2000 K.

#### F. Helium reconsidered

Above, we noticed in some cases a substantial disagreement between computed and observed spectral intensity distributions — especially for helium bubbles in freezing water. This defect is somewhat surprising, because the emitted photon numbers per flash certainly are in reasonable agreement with observation. We want to speculate here for a moment in which ways our simulations might have to be modified to obtain better consistency of computed and observed spectral profiles. The fact that our computed spectra lack intensity in

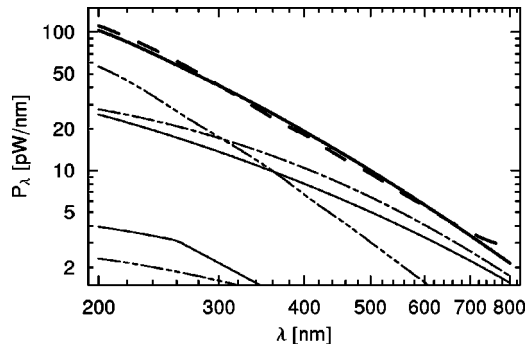


FIG. 3. Spectrum of a helium bubble in freezing water. For the computation it is assumed that the interior of the bubble with radius  $R'_{\min}=0.16 \mu\text{m}$  is heated to a maximum temperature of about 59 000 K. All radiative processes are indicated as in Fig. 1 above; the emission due to charge exchange and related processes, Eqs. (47) and (48), is indicated by the dash-triple-dotted line.

the ultraviolet seems to indicate that the actual source of light is probably hotter than what our model predicts. Yet, a hotter source will in general emit more photons, which would pose a new problem because presently computed and observed photon numbers are already consistent. One might therefore speculate that perhaps a smaller, but somewhat hotter part of the bubble contributes significantly to the light emission than is assumed in our model. We note that all estimates we were able to come up with indicate that the sonoluminescent source is reasonably transparent; the source is a volume emitter (as opposed to a black body, which is opaque and thus a surface emitter).

Thus we modified our program to crudely estimate the emission of a bubble with a nonuniform temperature profile. We assume that only a fraction of the bubble with radius  $R'(t) = a_R R(t)$  is sufficiently hot to emit light. Furthermore, the energy in the bubble is redistributed so that this core is heated to a higher, but uniform temperature than the average bubble temperature quoted above. Figure 3 shows the result of a computation where the light emitting region of the bubble of minimum radius  $R'_{\min}=0.16 \mu\text{m}$  is heated to a maximum temperature of about 59 000 K. Notice that now the emission due to helium charge exchange radiation, ion-atom bremsstrahlung, and radiative association, Eqs. (47) and (48), contributes substantially because of the significantly larger density of helium ions (however, note the discussion concerning  $\text{He}^+$  above, Sec. V E), compared to the homogeneous calculation. Excellent agreement with observation may thus be obtained.

We note that another possible scenario was suggested in Ref. [65]. The sonoluminescence spectra resemble black-body spectra. Indeed, the helium spectrum recorded in water at freezing temperature can be fitted to a black-body spectrum of about 25 000 K to 30 000 K. However, the radiative processes investigated in this paper are by far too weak to render a small source, such as the sonoluminescent bubble, opaque at these temperatures: to that end radiative processes would be required that are at least about 100 times more efficient than the processes known to us. In Fig. 4 we show the result of a calculation where the efficiency of electron-

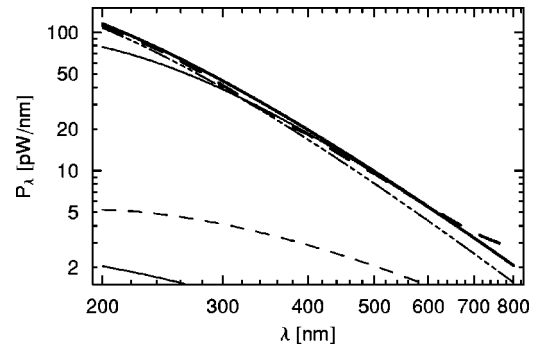


FIG. 4. Spectrum of a helium bubble in freezing water. For the computation it is assumed that the interior of the bubble with radius  $R'_{\min}=0.219 \mu\text{m}$  was heated to a maximum temperature of about 29 000 K and that some radiative process existed that is 100 times more efficient than electron-neutral bremsstrahlung and charge exchange radiation, thus rendering the bubble optically thick. All radiative processes are indicated as in Fig. 3.

neutral bremsstrahlung and charge exchange radiation was multiplied by 100 and the peak temperature in the light emitting region of minimum radius  $R'_{\min}=0.219 \mu\text{m}$  is 29 000 K. Agreement between observation and computation may obviously be obtained in this way. However, radiative processes of the required efficiency probably do not exist and only a density in the light emitting part that is a factor of 10 higher would render this region opaque, since the radiative processes are proportional to the density squared. Such a high density ( $>2000$  amagat), however, corresponds to a compression where the average distance between two helium atoms is only about 70% of the van der Waals hard sphere radius, which seems unrealistic.

Both, black body and hot ionized gas spectra reproduce measured spectral profiles quite well within the limits of uncertainties. Yet, since we are unaware of a radiative process that could provide for the significantly higher opacity, we favor the hot ionized gas model over the colder black-body model. In either case, the present considerations seem to suggest that a nonuniform temperature field in the bubble may be necessary to explain the observed helium spectra. Notice also that the spectra computed for the other rare gases in water at freezing temperatures seem to need such a nonuniform bubble heating as well, to a certain degree — more so than the spectra computed for water at room temperature. Yet, the spectra for cold water were obtained at higher driving pressure amplitudes, which should be more likely to cause some sort of inhomogeneous bubble heating than the milder pressures used at higher water temperatures. Also, the lighter the rare gas the more inhomogeneous heating seems to play a role.

We note that a possible reason for the nonuniform heating could be compression waves in the bubble launched by the rapid collapse. This subject was discussed, e.g., in Refs. [73,74]. While in these simulations [73,74] the bubble heats less inhomogeneously than it seems to be necessary from the present considerations, it is important to note that in the simulations [73,74] smaller driving pressure amplitudes were used than in the present paper and stronger driving causes more inhomogeneous heating [73,74].

## VII. SUMMARY AND CONCLUSIONS

We have constructed a model of sonoluminescent bubbles that contain a rare gas as well as water vapor. The vapor content varies during an acoustic cycle because of condensation and evaporation. Furthermore, dissociation and ionization reactions due to the varying temperatures and densities in the bubble are included. The degree of ionization of the ten species considered in our simulation is computed using ionization and recombination rate equations with realistic partition functions. For all species in the bubble, we compute emission from electron-neutral, electron-ion, and (for helium) ion-neutral bremsstrahlung, as well as recombination radiation. Furthermore, radiative attachment of electrons to oxygen and hydrogen atoms has been considered as well as polarization bremsstrahlung and, again for helium only, charge exchange radiation and radiative ion-atom association.

We have neglected in our model the light emission from OH and H<sub>2</sub>O molecules, which may be more or less important in multiple bubble sonoluminescence [66–69]. These processes will, however, not contribute at temperatures above 9000 K, since at such temperatures virtually all molecules have dissociated. In single bubble sonoluminescence, the theoretically suggested [70,71] and experimentally (indirectly) observed [72] mechanism of rare-gas rectification requires temperatures of about 9000 K [71]. Or, at least, the temperature to dissociate water molecules should be lower than the temperatures required to dissociate the triple bond of N<sub>2</sub>.

We find that the excluded volume van der Waals equation of state is the most useful simple equation of state for the given problem and that a fairly complete model of the water chemistry seems necessary.

Furthermore, the use of realistic partition functions is important for the computation of the degree of ionization; compared to the hydrogenlike atom model used previously a significant shift of the ionization balance to the ionized state results. Moreover, the various mechanisms that cause a lowering of the ionization potential increase ionization further. On the other hand, ionization is somewhat reduced when the energy losses due to ionization are accounted for. Furthermore, our results based on rate equation and those based on the Saha equation agree, a fact that suggests that thermal equilibrium with respect to ionization is obtained. Including

only the singly ionized state is sufficient; double ionization of the atoms and molecules is negligible.

The model presented here suggests that with decreasing driving frequencies bubble temperatures are limited, as was recently demonstrated in Ref. [17]; no upscaling of sonoluminescence emission may thus be expected when the driving frequencies are lowered.

We have also studied the emission of helium, argon, and xenon bubbles in water at freezing and room temperature. We find that the model correctly reproduces experimentally observed photon numbers and pulse widths, even for helium bubbles. The spectral shapes, however, tend to overemphasize the red while neglecting the ultraviolet. We find that in most cases the dominant radiation comes from the electron–rare-gas bremsstrahlung mechanisms and the radiative electron attachment to neutral hydrogen and oxygen atoms.

One possible explanation for the disagreement between computed and observed spectral intensity distributions may have to do with our assumption of an isotropic bubble, an assumption that should be taken with caution. Instead the bubble may be heated somewhat nonisotropically [73,74], which means that core parts will be hotter than the “average” temperature assumed here. Since, however, the ionization depends roughly exponentially on the temperature, emission will be dominated by the hotter parts of the bubble. Yet, the shape of the spectrum depends strongly on the temperature: hotter sources give more ultraviolet emission and less intensity in the red. We have shown in a crude approximation that inhomogeneous bubble heating indeed can account for the observed spectral intensity distributions. It is, however, also possible that some so far neglected radiative process strongly contributes to the emission in the ultraviolet. For example, excimer radiation or a related mechanism could be such a process: Excited rare-gas atoms may combine with a ground-state atom to form a diatomic molecule (“excimer”), which radiatively decays into its dissociative groundstate [9,75–78]. A more or less characteristic, continuous spectrum results with typically high intensities in the visible and ultraviolet range [78].

## ACKNOWLEDGMENTS

We thank M. Brenner, D. Lohse, B. Storey, and R. Toegel for stimulating discussions. The support of the Welch Foundation, Grant No. 1346, is gratefully acknowledged.

- 
- [1] D.F. Gaitan, L.A. Crum, C.C. Church, and R.A. Roy, *J. Acoust. Soc. Am.* **91**, 3166 (1992).
  - [2] *Cavitation and Inhomogeneities in Underwater Acoustics*, edited by W. Lauterborn (Springer, Berlin, 1980).
  - [3] F. R. Young, *Cavitation* (McGraw Hill, New York, N. Y., 1989).
  - [4] T.G. Leighton, *The Acoustic Bubble* (Academic Press, London, 1994).
  - [5] J.D.N. Cheeke, *Can. J. Phys.* **75**, 77 (1997).
  - [6] W. Lauterborn, in *Encyclopedia of Acoustics*, edited by M. J. Crocker (Wiley, New York, 1997), Vol. 1, Chap. 25, pp. 263–270.
  - [7] B.P. Barber *et al.*, *Phys. Rep.* **281**, 65 (1997).
  - [8] J.R. Blake, *Philos. Trans. R. Soc. London, Ser. A* **357**, 200ff (1999), special issue devoted to sonoluminescence.
  - [9] D. Hammer and L. Frommhold, *J. Mod. Opt.* **48**, 239 (2001).
  - [10] M.P. Brenner, S. Hilgenfeldt, and D. Lohse, *Rev. Mod. Phys.* (to be published).
  - [11] K. Yasui, *Phys. Rev. E* **56**, 6750 (1997).
  - [12] S. Hilgenfeldt, S. Grossmann, and D. Lohse, *Phys. Fluids* **11**, 1318 (1999).
  - [13] D. Hammer and L. Frommhold, *Phys. Fluids* **12**, 472 (2000).
  - [14] K. Yasui, *Phys. Rev. E* **60**, 1754 (1999).

- [15] D. Hammer and L. Frommhold, Phys. Rev. Lett. **85**, 1326 (2000).
- [16] S. Hilgenfeldt and D. Lohse, Phys. Rev. Lett. **82**, 1036 (1999).
- [17] R. Toegel, B. Gompf, R. Pecha, and D. Lohse, Phys. Rev. Lett. **85**, 3165 (2000).
- [18] A. Prosperetti and A. Lezzi, J. Fluid Mech. **168**, 457 (1986).
- [19] C. E. Brennen, *Cavitation and Bubble Dynamics* (Oxford University Press, Oxford, 1995).
- [20] V. Kamath, A. Prosperetti, and F.N. Eglolfopoulos, J. Acoust. Soc. Am. **94**, 248 (1993).
- [21] R. W. Schrage, *A Theoretical Study of Interphase Mass Transfer* (Columbia University Press, New York, 1953).
- [22] S. Fujikawa and T. Akamatsu, J. Fluid Mech. **97**, 481 (1980).
- [23] J. A. Fay, *Molecular Thermodynamics* (Addison-Wesley, Reading, MA, 1965).
- [24] D. Mihalas, *Stellar Atmospheres* (Freeman, San Francisco, 1978).
- [25] D. E. Post *et al.*, At. Data Nucl. Data Tables **20**, 297 (1977).
- [26] N. Xu, L. Wang, and X. Hu, Phys. Rev. E **57**, 1615 (1998).
- [27] NIST, 2001, database at <http://physics.nist.gov/PhysRefData/IonEnergy/ionEnergy.html>
- [28] A.W. Irwin, Astrophys. J., Suppl. Ser. **45**, 621 (1981).
- [29] A.J. Sauval and J.B. Tatum, Astrophys. J., Suppl. Ser. **56**, 193 (1984).
- [30] E. Fermi, Nuovo Cimento **11**, 1934 (1934).
- [31] H. Griem, *Principles of Plasma Spectroscopy* (Cambridge University Press, New York, 1997).
- [32] N. Allard and J. Kielkopf, Rev. Mod. Phys. **54**, 1103 (1982).
- [33] A. Royer, Phys. Rev. A **22**, 1625 (1980).
- [34] P. Fromy, C. Deutsch, and G. Maynard, Phys. Plasmas **3**, 714 (1996).
- [35] P. Laporte, V. Saile, R. Reininger, U. Asaf, and I.T. Steinberger, Phys. Rev. A **28**, 3613 (1983).
- [36] N. Bonifaci, A. Denat, and V. Atrazhev, J. Phys. D **30**, 2717 (1997).
- [37] J.A. Hornbeck and J.P. Molnar, Phys. Rev. **84**, 621 (1951).
- [38] J. Stein and D. Salzmann, Phys. Rev. A **45**, 3943 (1992).
- [39] A.M. Ermolaev, A.A. Mihajlov, L.M. Ignjatović, and M.S. Dimitrijević, J. Phys. D **28**, 1047 (1995).
- [40] V.A. Astapenko, L.A. Bureyeva, and V.S. Lisitsa, J. Exp. Theor. Phys. **90**, 434 (2000).
- [41] *Polarization Bremsstrahlung*, edited by V. N. Tsytovich and I. M. Ojringel (Plenum, New York, 1992).
- [42] D. Hammer and L. Frommhold, Phys. Rev. A **64**, 024705 (2001).
- [43] Y. B. Zel'dovich and Y. P. Raizer, *Physics of Shock Waves and High Temperature Hydrodynamic Phenomena* (Academic Press, New York, 1966), Vol. 1.
- [44] L. Frommhold, Phys. Rev. E **58**, 1899 (1998).
- [45] S. Geltman, J. Quant. Spectrosc. Radiat. Transf. **13**, 601 (1973).
- [46] A. Unsöld, *Physik der Sternatmosphären* (Springer, Berlin, 1955).
- [47] R. Fuchs, Z. Phys. **130**, 69 (1951).
- [48] W. Lochte-Holtgreven and H. Maecker, Z. Phys. **38**, 258 (1951).
- [49] J. Keck, J. Camm, and B. Kivel, J. Chem. Phys. **28**, 723 (1958).
- [50] J. Keck, J. Camm, B. Kivel, and T. WentinK,Jr., Ann. Phys. (N.Y.) **7**, 1 (1959).
- [51] L. M. Branscomb, in *Atomic and Molecular Processes*, edited by D. R. Bates (Acad. Press, New York, 1962), pp. 100–140.
- [52] J. N. Bradley, *Shock Waves in Chemistry and Physics* (Methuen, London, 1962).
- [53] S. Geltman, Astrophys. J. **136**, 935 (1962).
- [54] *Atomic and Molecular Processes*, edited by D. R. Bates (Acad. Press, New York, 1962).
- [55] The experimental photon number was obtained by numerically integrating the spectra shown for the different rare gases in water at 0 °C and 20 °C in Ref. [7]. The photon numbers computed in this way were then divided by  $4\pi$  since this factor was reported to be missing in plots of measured spectral intensity later [79,65].
- [56] B.D. Storey and A.J. Szeri, Proc. R. Soc. London **456**, 1685 (2000).
- [57] B. Gompf *et al.*, Phys. Rev. Lett. **79**, 1405 (1997).
- [58] R.A. Hiller, S.J. Putterman, and K.R. Weninger, Phys. Rev. Lett. **80**, 1090 (1998).
- [59] B.P. Barber *et al.*, Phys. Rev. Lett. **72**, 1380 (1994).
- [60] S. Hilgenfeldt, D. Lohse, and W.C. Moss, Phys. Rev. Lett. **80**, 1332 (1998); **80**, 3164 (1998).
- [61] S. Hilgenfeldt, S. Grossmann, and D. Lohse, Nature (London) **398**, 402 (1999).
- [62] G. C. Maitland, M. Rigby, E. B. Smith, and W. A. Wakeham, *Intermolecular Forces* (Clarendon Press, Oxford, 1981).
- [63] R.A. Aziz, J. Chem. Phys. **99**, 4518 (1993).
- [64] J. O. Hirschfelder, C. F. Curtiss, and R. B. Bird, *Molecular Theory of Gases and Liquids* (Wiley, New York, 1954).
- [65] G. Vazquez, C. Camara, S. Putterman, and K. Weninger, Opt. Lett. **26**, 575 (2001).
- [66] Y.T. Didenko, W.B. McNamara, and K.S. Suslick, J. Phys. Chem. A **103**, 10 783 (1999).
- [67] C. Sehgal, R.G. Sutherland, and R.E. Verrall, J. Phys. Chem. **84**, 388 (1980).
- [68] T.K. Saksena and W.L. Nyborg, J. Chem. Phys. **53**, 1722 (1970).
- [69] Y.T. Didenko and S.P. Pugach, J. Phys. Chem. **98**, 9742 (1994).
- [70] D. Lohse *et al.*, Phys. Rev. Lett. **78**, 1359 (1997).
- [71] D. Lohse and S. Hilgenfeldt, J. Chem. Phys. **107**, 6986 (1997).
- [72] J.A. Ketterling and R.E. Apfel, Phys. Rev. Lett. **81**, 4991 (1998).
- [73] V.Q. Vuong and A.J. Szeri, Phys. Fluids **8**, 2354 (1996).
- [74] V.Q. Vuong, A.J. Szeri, and D.A. Young, Phys. Fluids **11**, 10 (1999).
- [75] Y. Tanaka and M. Zelikoff, J. Opt. Soc. Am. **44**, 254 (1954).
- [76] Y. Tanaka, J. Opt. Soc. Am. **45**, 710 (1955).
- [77] P.G. Wilkinson and Y. Tanaka, J. Opt. Soc. Am. **45**, 344 (1955).
- [78] J. Tellinghuisen, in *Applied Atomic Collision Physics*, edited by E. W. McDaniel and W. L. Nighan (Academic Press, New York, 1982), Vol. 3, Chap. 9, pp. 251–271.
- [79] K.R. Weninger, C.G. Camara, and S.J. Putterman, Phys. Rev. E **63**, 016310 (2001).